Applied Mathematical Modelling 39 (2015) 667–681

Contents lists available at ScienceDirect

Applied Mathematical Modelling

journal homepage: www.elsevier.com/locate/apm

Inverse solutions of temperature, heat flux and heat source by the Green element method

Akpofure E. Taigbenu

School of Civil and Environmental Engineering, University of the Witwatersrand, P. Bag 3, Johannesburg WITS 2050, South Africa

ARTICLE INFO

Article history:
Received 11 July 2013
Received in revised form 22 May 2014
Accepted 30 June 2014
Available online 10 July 2014

Keywords:
Inverse temperature
Heat flux and heat source recovery
Green element method
Singular value decomposition
Tikhonov regularization

ABSTRACT

In two spatial dimensions, inverse heat conduction problems of temperature, heat flux and heat source recovery are solved in homogeneous and heterogeneous media for steady and transient cases by the Green element method (GEM). The formulation of GEM employed is presented in Taigbenu (2012) [27] and it uses a second-order difference expression to approximate the internal normal fluxes and, therefore, gives accuracy comparable to the flux-based formulation. The Tikhonov regularization with the singular value decomposition (SVD) are used to solve in a least square sense the over-determined, ill-conditioned discrete equations arising from the element-by-element implementation of the singular integral equations. With seven numerical examples, the numerical characteristics of the GEM are evaluated for inverse problems where it is required to recover the temperature, heat flux and heat source from available data. In some of the examples, the performance of the formulation is evaluated when random errors are introduced into the measured data. Excellent results are obtained from the simulated numerical examples, and more especially that these results are obtained with coarse grids.

1. Introduction

The inverse heat conduction problem (IHCP) arises in many practical applications in the fields of science and engineering where the transport of heat, mass and energy takes place in natural and man-made materials. There are various classes of IHCPs which range from recovery of boundary temperature and heat flux [1–6], estimation of medium parameters [7–10], recovery of the spatial and temporal distributions of heat sources/sinks [11–19], recovery of initial data distributions [11,20–22], and recovery of the shape and location of boundary and medium features [23–26]. In most instances sensor measurements of temperature and heat fluxes are available at some accessible parts of the domain to support the solution of the IHCPs. In this work, the first and third classes of IHCPs, earlier alluded to, are addressed. Unlike the direct problem which gives a unique solution and whose numerical solution gives rise to a coefficient matrix that is well conditioned, the inverse problem might yield non-unique solutions and the coefficient matrix, arising from its numerical discretization, is usually ill-conditioned. The degree of ill-conditioning depends to a large extent on the distribution of the available data in relation to the solution being sought.

Many numerical methods – the finite difference method (FDM), the finite element method (FEM) and the boundary element method (BEM), and their variants – have been applied to IHCPs, and this is evident from the numerous references that are available in the literature. This is the first time GEM, a variant of BEM, is being applied to these classes of problems. It

E-mail address: akpofure.taigbenu@wits.ac.za

http://dx.doi.org/10.1016/j.apm.2014.06.020
0307-904X/

is based on the formulation of the GEM that was recently derived by Taigbenu [27] in which a second-order polynomial expression is used to approximate the internal normal fluxes so that only the solution for the temperature or the flux is calculated at external nodes and the temperature at internal nodes. This formulation was shown to exhibit comparable accuracy as the flux-based formulation, and also readily lends itself to solving inverse problems. The resultant coefficient matrix from applying this formulation to the IHCP is ill-conditioned, and it is handled by the SVD method with Tikhonov regularization. The current GEM formulation is tested with four examples of the class of IHCP which deals with recovery of temperature and heat fluxes, and three examples of recovery of the strength of the heat sources which are assumed to be time dependent. All of the numerical examples are solved by GEM with coarse 2-D spatial discretization of the domain, which is indicative of the accuracy of the formulation. The ability of GEM to address this wide range of IHCPs demonstrates the robustness of the current formulation in addressing inverse problems.

2. Governing equation

The IHCP addressed in this paper is governed by the differential equation

$$\nabla \cdot [K\nabla T] = \rho c \frac{\partial T}{\partial t} + Q(t), \tag{1}$$

where $\nabla = \mathbf{i}\partial/\partial x + \mathbf{j}\partial/\partial y$ is the 2-D gradient operator with the spatial variables x and y, t is the time dimension, T is the temperature field, K is the thermal conductivity, ρ is the density, c is the specific heat capacity, and Q represents heat sources and sinks that are assumed to have only temporal variation. Eq. (1) applies to a domain Ω over which the specified initial condition is

$$T(x, y, t = 0) = T_0(x, y). \tag{2a}$$

The conditions specified on the boundary Γ are:

$$T(x, y, t) = T_1 \text{ on } \Gamma_1, \tag{2b}$$

$$-K\nabla T \cdot \mathbf{n} = q_2 \text{ on } \Gamma_2, \tag{2c}$$

$$T(x, y, t) = T_3 \text{ and } -K\nabla T \cdot \mathbf{n} = q_3 \text{ on } \Gamma_3, \tag{2d}$$

where $\mathbf{n}$ is the unit outward pointing normal on the boundary. Two types of IHCP problems are addressed in this paper; the first requires the calculation of the solution for the temperature T and heat flux q on a part of the boundary, denoted Γ_4, and the second seeks the recovery of the strength of the heat source over time. In both types of problems, measurements of the temperature may be available at specified internal points in the domain. The measured temperature value at any internal point (x_m, y_m) is denoted as $T_m = T(x_m, y_m, t)$, with N_i available sensor measurements. Fig. 1 shows the domain Ω with boundary $\Gamma = \Gamma_1 \cup \Gamma_2 \cup \Gamma_3 \cup \Gamma_4$. When the boundary Γ_4 does not exist and $Q(t)$ is known, the problem reduces to the direct one which is solved without requiring information on the temperature at internal points. For the solution of inverse problems to be possible, the number of discrete equations that are generated by GEM has to be equal to or greater than the number of unknowns.

The heat sources can be uniformly distributed and/or point sources. For the latter, they are represented as

$$Q(t) = \sum_{n=1}^{P} Q_n \delta(r - r_n), \tag{3}$$

where Q_n is the strength of the nth heat source located at $r_n = (x_n, y_n)$, P is the number of these point heat sources, and $\delta(r - r_i)$ is the Dirac delta function. Eq. (1) can be expressed as a Poisson equation that is given by

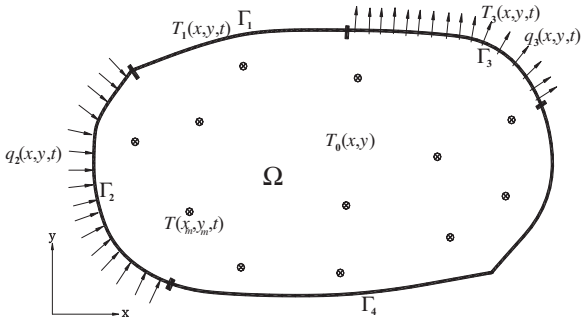

Fig. 1. Domain and problem statement representation.

$$\nabla^2 T = -\nabla\Psi\cdot\nabla T + \Phi\frac{\partial T}{\partial t} + \varphi Q, \tag{4}$$

where $\Psi = \ln K$ is dimensionless, and this is achieved by normalizing K with a unit value of the thermal conductivity that has the same dimensional units as K, $\Phi = \rho c/K$ is the reciprocal of the thermal diffusivity, and $\varphi = 1/K$. Applying Green's theorem to Eq. (4) results in its integral equation that is given by

$$-\lambda T_i + \int_\Gamma (T\nabla G\cdot\mathbf{n} + G\varphi q)dS + \iint_\Omega G[-\nabla\Psi\cdot\nabla h + \Phi\frac{\partial T}{\partial t} + \varphi Q]\,dA = 0, \tag{5}$$

where $G = \ln(r - r_i)$ is the fundamental solution of $\nabla^2 G = \delta(r - r_i)$ in the infinite domain, $q = -K\nabla T\cdot\mathbf{n}$ is the normal heat flux, the subscript i denotes the source or collocation node $r_i = (x_i, y_i)$ and λ is the nodal angle at r_i obtained from the Cauchy part of the integration of the Dirac delta function $\delta(r - r_i)$ at the source node. The boundary and domain integrals in Eq. (5) are implemented in the Green element sense over sub-domains or elements that are used to discretize the computational domain. This, in essence, is a limiting case of the domain decomposition technique in which the element arrangement is similar to that of finite elements [28,29]. On these elements, Lagrange-type interpolations are prescribed for T, φq and Ψ, that is $T \approx N_j T_j$ (N_j are the interpolation functions which, in this paper, are chosen to be linear). Introducing the interpolation relationship into Eq. (5) results in the discrete element equations applicable to each sub-domain or element denoted as Ω^e. That is

$$R_{ij}T_j + L_{ij}(\varphi q)_j - U_{imj}\Psi_m T_j - V_{imj}\Psi_m T_j + W_{imj}\Phi_m\frac{dT_j}{dt} + F_{ij}Q_j = 0, \tag{6}$$

where

$$R_{ij} = \int_{\Gamma^e} N_j\nabla G_i\cdot\mathbf{n}\,ds - \delta_{ij}\lambda, \quad L_{ij} = \int_{\Gamma^e} N_j G_i ds, \quad U_{imj} = \iint_{\Omega^e} G_i\frac{\partial N_m}{\partial x}\frac{\partial N_j}{\partial x}\,dA, \quad V_{imj} = \iint_{\Omega^e} G_i\frac{\partial N_m}{\partial y}\frac{\partial N_j}{\partial y}\,dA,$$
$$W_{imj} = \iint_{\Omega^e} G_i N_m N_j\,dA. \tag{7}$$

In Eq. (7), Γ^e is the boundary of the elemental domain Ω^e and δ_{ij} is the Kronecker delta. All these integrations are evaluated analytically on linear rectangular and triangular elements. The expression for the matrix F_{ij}, resulting from the contribution of heat sources, depends on whether they are distributed or point sources. For distributed sources, it has the expression

$$F_{ij} = \varphi(r_j)\iint_{\Omega^e}\ln(r - r_i)N_j\,dA, \tag{8a}$$

and for each point source, the expression is

$$F_{ij} = \varphi(r_j)\ln(r_j - r_i), \tag{8b}$$

where $\varphi(r_j)$ is the reciprocal of the thermal conductivity that is evaluated at $r_j = (x_j, y_j)$. The discrete element Eq. (6) is aggregated for all the elements that are employed in discretizing the computational domain. The outcome for doing this is the matrix equation

$$E_{ij}T_j + B_{ij}q_j + C_{ij}\frac{dT_j}{dt} + F_{ij}Q_j = 0, \tag{9}$$

where $E_{ij} = R_{ij} - U_{imj}\Psi_m - V_{imj}\Psi_m$, $B_{ij} = L_{im}\varphi\delta_{mj}$ and $C_{ij} = W_{imj}\Phi_m$. The formulation presented in Taigbenu [27] is used to approximate the normal flux q at inter-element boundaries. It approximates q in terms of T which is represented by a quadratic polynomial of the spatial variables $r = (x, y)$. As earlier demonstrated, this formulation greatly improves the accuracy of the numerical solutions to a level that is comparable to the flux-based GEM [30,31]. With this approximation, calculations are required for T and q on the boundary of the computational domain and T at nodes within the domain. The temporal derivative term is approximated by a finite difference expression: $dT/dt \approx [T^{(2)} - T^{(1)}]/\Delta t$ evaluated at $t = t_1 + \beta\Delta t$, where $0 \leqslant \beta \leqslant 1$, is the difference weighting factor, and Δt is the time step between the current time t_2 and the previous one t_1. Introducing the approximation for the temporal derivative in Eq. (9) and weighting the other terms by β yields

$$\left(\beta E_{ij} + \frac{C_{ij}}{\Delta t}\right)T_j^{(2)} + \beta B_{ij}q_j^{(2)} + \beta F_{ij}Q_j^{(2)} = \left(\omega E_{ij} + \frac{C_{ij}}{\Delta t}\right)T_j^{(1)} + \omega B_{ij}q_j^{(1)} + \beta F_{ij}Q_j^{(1)}, \tag{10}$$

where $\omega = \beta - 1$ and the bracketed superscripts represent the times at which the quantities are evaluated. The initial and boundary data and available internal temperature measurements are incorporated into Eq. (10) to give the matrix equation

$$\mathbf{Ap} = \mathbf{b}, \tag{11}$$

where

$$\mathbf{A} = \begin{bmatrix} \beta E_{ij} + \frac{C_{ij}}{\Delta t} \\ \beta B_{ij} \\ \beta F_{ij} \end{bmatrix} \quad \text{and} \quad \mathbf{p} = \begin{Bmatrix} T_j^{(2)} \\ q_j^{(2)} \\ Q_j^{(2)} \end{Bmatrix}, \tag{12}$$

where $\mathbf{p}$ is an $N \times 1$ vector of unknowns (T and/or q at external nodes, T at internal nodes and the heat sources, Q). The matrix $\mathbf{A}$ is an $M \times N$ matrix, where M is the number of nodes in the computational domain (which equals the number of discrete equations generated by the GEM formulation) and $M \geqslant N$, and $\mathbf{b}$ is an $M \times 1$ vector of known quantities which consist of the terms on the right hand side of Eq. (10) and as well as the contributions from the available temperature measurements. Eq. (11) is over-determined and generally ill-conditioned system of equations that can be solved by the least square method with regularization. The singular value decomposition (SVD) method is used to facilitate the decomposition of the $M \times N$ matrix $\mathbf{A}$ by the relationship [32]

$$\mathbf{A} = \mathbf{U}\mathbf{D}\mathbf{V}^t = \sum_{i=1}^{N} \psi_i u_i v_i^{tr}, \tag{13}$$

where $\mathbf{U}$ is an $M \times M$ matrix and $\mathbf{V}$ is an $N \times N$ matrix; both are orthogonal square matrices, and $\mathbf{D}$ is an $M \times N$ diagonal matrix with N non-negative diagonal elements ($\mathbf{D} = diag(\psi_1, \psi_2, \ldots, \psi_N)$) which satisfy the condition: $\psi_1 > \psi_2 > \cdots > \psi_N > 0$. N is the rank of the matrix $\mathbf{A}$, and u_i and v_i are the ith column of the matrices $\mathbf{U}$ and $\mathbf{V}$, respectively. By the least square solution of Eq. (11), the Euclidian norm $||\mathbf{A}\mathbf{p} - \mathbf{b}||^2$ is minimized to give the solution for the unknowns $\mathbf{p}$

$$\mathbf{p} = \mathbf{B}^{-1}\mathbf{s}, \tag{14}$$

where $\mathbf{B} = \mathbf{A}^{tr}\mathbf{A}$ is an $N \times N$ matrix, and $\mathbf{s} = \mathbf{A}^{tr}\mathbf{b}$ is an $N \times 1$ vector. Introducing the expression for $\mathbf{A}$ from Eq. (13) into Eq. (14) gives

$$\mathbf{p} = \sum_{i=1}^{N} \frac{u_i^{tr}\mathbf{b}}{\psi_i} v_i. \tag{15}$$

The small singular values ψ_i cause instability of the solution for $\mathbf{p}$ by Eq. (15), and for that reason, either regularization is carried out or the singular values less than a prescribed threshold are truncated. The former approach is the regularized SVD approach, while the latter is the truncated SVD. The former is followed in this work. The Tikhonov regularization method, one of the earliest regularization methods, is used in this work. It is a smoothening technique that attempts to stabilize the numerical results from solving the ill-conditioned system of equations of the IHCP problem [33]. The Tikhonov regularization technique minimizes $||\mathbf{A}\mathbf{p} - \mathbf{b}||^2 + \alpha^2||\mathbf{I}\mathbf{p}||^2$, resulting in the solution for $\mathbf{p}$ that is given by ($\mathbf{I}$ is the identity matrix)

$$\mathbf{p}(\alpha) = \sum_{i=1}^{N} \frac{\psi_i}{\alpha^2 + \psi_i^2} u_i^{tr}\mathbf{b} v_i, \tag{16}$$

where α is the regulation parameter. The factor $\psi_i/(\alpha^2 + {\psi_i}^2)$ in Eq. (16) serves to dampen the contribution of the small singular values. The choice of α has to be carefully done so that it is not too small to retain the instability of the numerical solution or too large to have smooth solutions that do not reflect the physics of the problem being addressed. As suggested by Hansen [34], we found, normalizing the singular values with the largest one ψ_1 such that $\psi_N < \cdots < \psi_2 < \psi_1 \leqslant 1$, to be useful in constraining the choice of the regularization parameter to that of the order of magnitude of the small singular values.

3. Numerical examples

Seven examples are used to assess the accuracy of the inverse formulation of the GEM earlier presented. The first two examples are non-transient, and one of them addresses heat conduction in a non-homogeneous medium. These examples had previously been addressed by the local integral equation (LIE) formulation of Sladek et al. [4]. The third and fourth examples are transient IHCPs. In these first four examples, the recovery of temperature and heat flux data is sought. The last three examples examine the recovery of the strength of heat sources under transient conditions and were addressed by Yan et al. [13] using the method of fundamental solutions (MFS). Using these seven examples provides a comprehensive assessment of the performance and robustness of the current GEM formulation in solving inverse heat conduction problems.

3.1. Example 1

Inverse heat conduction under steady condition is examined in a square medium $[1 \times 1]$ with material properties that are homogeneous but slightly different from those used by Sladek et al. [4] who solved a similar example. The thermal conductivity $K = 1$ and there is no heat source in the medium, $Q = 0$. The exact solution for this test example that satisfies the governing equation is $T = y$. Three cases of boundary conditions, presented in Fig. 2a–c, are evaluated. In case (i), zero heat flux and a linear temperature variation with y are prescribed on the right boundary, while no data on T and q are available on the other three boundaries which are, therefore, Γ_4 boundaries. Temperature measurements are available at 19 internal points (along $x = 0.125$, $y = 0.125$ and $y = 0.875$), and indicated by the empty circles in Fig. 2a. In case (ii), the left and right boundaries are insulated, while unit temperature and unit heat flux are specified on the top boundary. The bottom boundary is a Γ_4 boundary where T and q are not known. No temperature measurements are available within the domain (Fig. 2b). Case (iii) has unit temperature specified on the top boundary, a linear temperature distribution and zero heat flux along the right

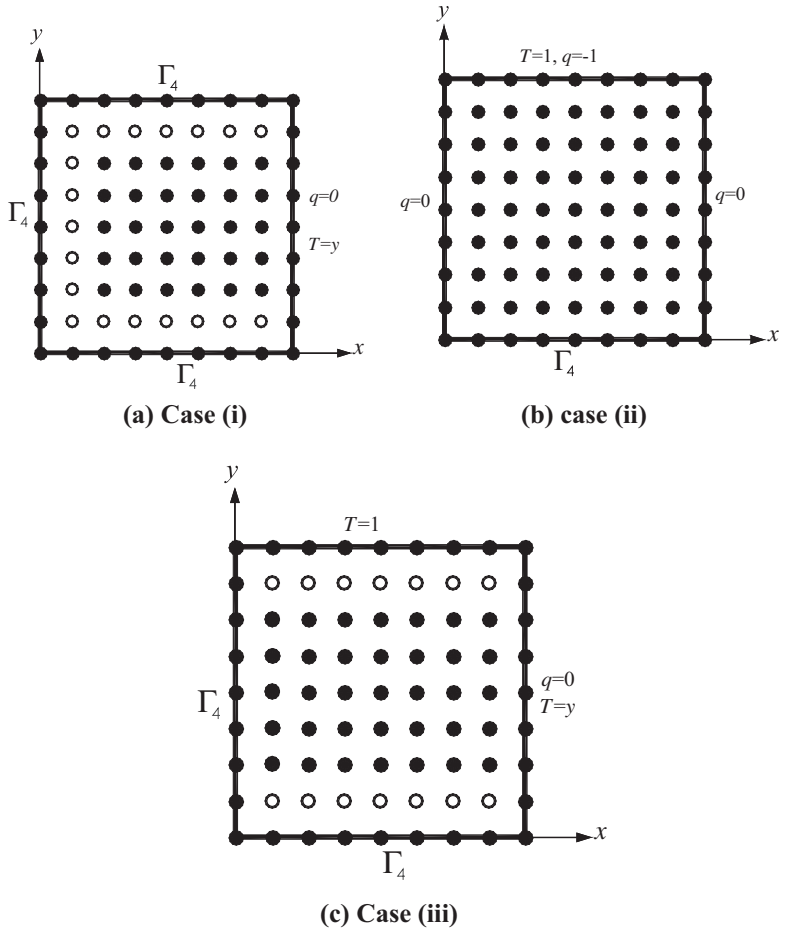

Fig. 2. Problem domain for three cases of Example 1.

boundary, and no boundary data on the left and bottom boundaries. 14 internal temperature measurements are available along $y = 0.125$ and $y = 0.875$ (Fig. 2c).

Using a grid of 8×8 linear rectangular elements with 32 boundary nodes and 49 internal nodes, numerical simulations are carried out with the GEM using the regularized SVD method to evaluate the ill-conditioned and over-determined system of equations. The relative error for the simulated temperature field is evaluated by the relationship

$$\varepsilon = \frac{\|T^{cal} - T^{exact}\|}{\|T^{exact}\|} \times 100, \tag{17}$$

where

$$\|T\| = \left(\iint_{\Omega} T^2 dA \right)^{1/2}. \tag{18}$$

The relative errors for the predicted temperature field by the GEM are compared in Table 1 to those of the LIE formulation of Sladek et al. [4] who used twice the number of boundary nodes of GEM. It is worth noting that while the accuracies of the two numerical solutions are comparable, it is achieved by GEM with fewer boundary nodes. It is only along the Γ_4 boundary that GEM results are presented for the temperature and the heat flux. These results for case (i) are presented in Fig. 3a and b, for case (ii) in Fig. 4a and b, and for case (iii) in Fig. 5a and b. In all the examples, there is better prediction of the temperature than the heat flux.

The influence of measurement errors, which do arise in practical situations, is also examined with these three cases of Example 1. To do so, the prescribed data for the temperature on the boundary and within the domain are perturbed in a random manner by the relationship

$$\tilde{T}_m = T_m[1 + \sigma \times RN(m)], \tag{19}$$

Table 1
Errors from the numerical simulations of Example 1.

Numerical method	Case (i)		Case (ii)		Case (iii)	
	Regulari-zation value, α	Relative error, ε	Regulari-zation value, α	Relative error, ε	Regulari-zation value, α	Relative error, ε
GEM (SVD)	5×10^{-4}	8.91×10^{-4}	10^{-5}	3.77×10^{-3}	3×10^{-9}	9.69×10^{-5}
LIE (SVD)		7.60×10^{-4}		2.50×10^{-3}		Not available

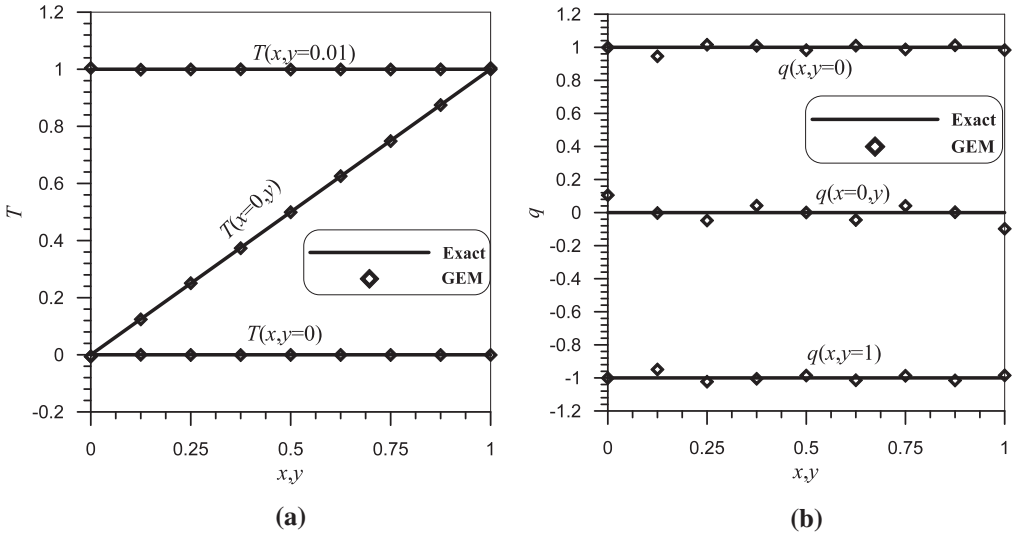

Fig. 3. Numerical solutions of the temperature and flux along the Γ_4 boundaries for case (i) Example 1.

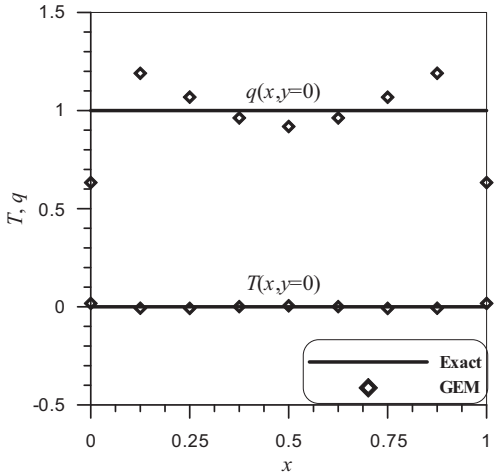

Fig. 4. Numerical solutions of the temperature and flux along the Γ_4 boundaries for case (ii) Example 1.

where σ denotes the magnitude of the error or noise level and $RN \in [-1, 1]$ are random numbers that are generated with the IMSL program routine RNNOR. Fig. 6a shows the variation of the relative error, ε, calculated by Eq. (17), with noise levels of 1%, 3% and 5% for the three cases of Example 1. Noting that the calculation of ε takes into account only the temperature field, we then examined how the noise in the data affects both the temperature field and heat flux. Using only case (i) of Example 1 (similar results were obtained for the other two cases), the influence of noise on the data was evaluated along the Γ_4 boundaries. The numerical errors, based on the root mean square error (RMSE), are presented in Fig. 6b. We observe greater influence of data noise on the GEM solution for the heat flux than the temperature. This is a typical experience with inverse

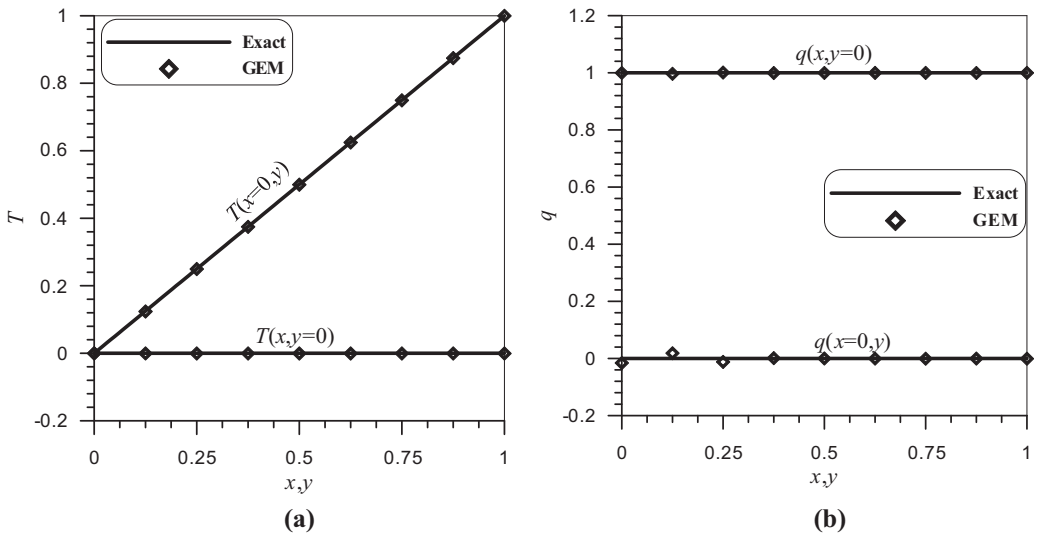

Fig. 5. Numerical solutions of the temperature and flux along the Γ_4 boundaries for case (iii) Example 1.

numerical simulations in which the influence of noise on the temperature T (primary field variable) is generally amplified on the heat flux q (secondary variable) [5,6,35].

In these three cases of Example 1 we have the benefit of the exact solution to benchmark the GEM solution with respect to choosing the value of the regularization parameter α. In most instances an exact solution is not available. Using case (i) of Example 1, comparison is made between the values of α that are chosen by making use of the available exact solution for which ε, obtained from Eq. (17), is minimized, and that based on the L-curve [34,36–38]. The L-curve is a plot of $||\mathbf{Ip}||^2$ versus the residual $||\mathbf{Ap} - \mathbf{b}||^2$ for all values of the regularization parameter α, with the corner of the plot reflecting the best compromise between these two quantities. The L-curve for case (i) of Example 1 with noise levels of σ = 0%, 1%, 3% and 5% is presented in Fig. 7. Comparing the values α obtained making use of the exact solution and that by the L-curve, presented in Table 2, indicates that the α values from the former are slightly higher than those of the latter. These discrepancies can be attributed to the fact that the optimum values of α that are based on the exact solution make use of only the calculated temperatures **T**, while those based on the L-curve use both the temperature and heat flux, $\mathbf{p} = \{\mathbf{T}, \mathbf{q}\}^{tr}$.

3.2. Example 2

In this example, the boundary conditions presented for case (iii) of Example 1 are considered. Following Sladek et al. [4], the thermal conductivity K varies exponentially with respect to the spatial variable y. That is

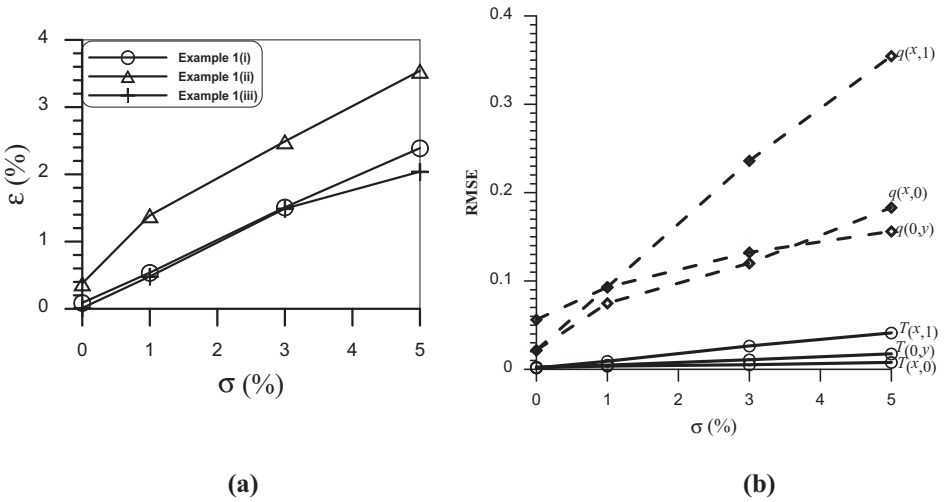

Fig. 6. Influence of data noise on the GEM solutions: (a) relative error versus noise, (b) RMSE versus noise along Γ_4 boundary for Example 1 (i).

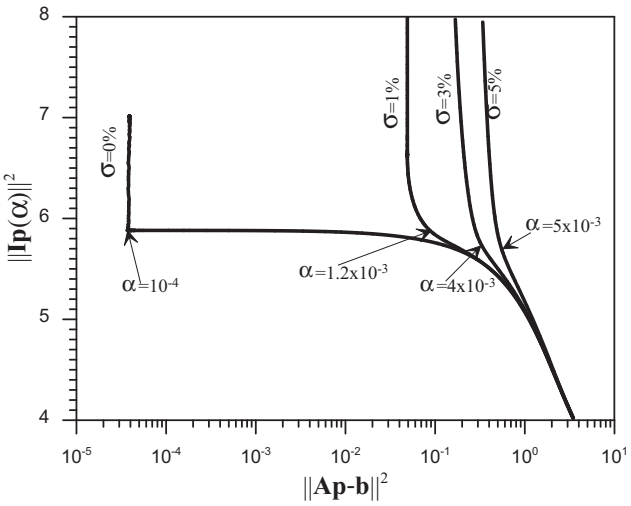

Fig. 7. The L-curve plot for case (i) of Example 1 at various noise levels.

Table 2
Optimum regularization parameter values using the exact solution and the L-curve for case (i) of Example 1.

Noise level σ (%)	Optimum α using the exact solution	α from L-curve
0	5×10^{-4}	10^{-4}
1	2×10^{-3}	1.2×10^{-3}
3	4×10^{-3}	4×10^{-3}
5	7×10^{-3}	5×10^{-3}

$$K = K_0 e^{\lambda y}, \tag{20}$$

where $K_0 = 1$, and two values of the parameter λ are used in the numerical simulations: $\lambda = 0.2$ and $\lambda = 0.5$. The exact solution is

$$T = \frac{e^{-\lambda y} - 1}{e^{-\lambda} - 1}. \tag{21}$$

As with Example 1, the GEM simulations are carried out with 8×8 linear rectangular grid, comprising 32 boundary nodes and 49 internal nodes. The relative error ε of the GEM solution of this example is compared to that of the LIE formulation of Sladek et al. [4] in Table 3 for two values of the exponents $\lambda = 0.2$ and $\lambda = 0.5$. With half the number of boundary nodes used in the LIE formulation, the GEM solutions are superior to those of the LIE. The GEM solutions along the left and bottom Γ_4 boundaries, where both T and q are unspecified, are presented in Fig. 8a and b for the case of $\lambda = 0.2$ and Fig. 9a and b for the case $\lambda = 0.5$. The results show that GEM gives good prediction of the temperature, T and boundary normal heat flux, q.

3.3. Example 3

This example is a transient IHCP that had previously been used as a test case by other authors [2,6]. Although it is one-dimensional in space, the GEM simulations are done in a rectangular 2-D domain with insulated boundaries at the top and bottom. The medium is homogeneous with $K = 1$ and no heat sources, $Q = 0$. With a test function $T(x, t) = 2t + x^2$ that satisfies the governing equation (1) in a domain $x \in [0, 1]$, the temperature distribution $T(x, 0) = x^2$ is prescribed at the initial time $t = 0$ and an Γ_3 boundary along $x = 1$ where the temperature and flux are specified, that is

Table 3
Errors from the numerical simulations of Example 2.

Numerical method	$\lambda = 0.2$		$\lambda = 0.5$	
	Regularization value, α	Relative error, ε	Regularization value, α	Relative error, ε
GEM	2×10^{-4}	7.90×10^{-4}	3×10^{-4}	9.26×10^{-4}
LIE		6.40×10^{-3}		1.30×10^{-2}

$$T(1,t)+q(1,t)=2t+3. \tag{22}$$

The boundary along $x=0$ is a Γ_4 boundary where neither T nor q is specified, and three cases of locations with available temperature measurements are examined: case (i) $x_m=1$, case (ii) $x_m=0.5$ and case (iii) $x_m=0.25$. The GEM simulations of this example used only four rectangular elements, a time step, $\Delta t=0.025$ and the fully implicit time differencing scheme, $\beta=1$. To minimize the influence of the imposed insulated top and bottom boundaries on the solution for this 1-D problem, the boundaries are kept as far apart from each other in the y direction. Arbitrarily the y dimension is set at 10^3. The values of the regularization parameter, obtained by employing the available analytical solution, for the three cases are: $\alpha=2.2\times10^{-4}$ for $x_m=1$, $\alpha=3\times10^{-3}$ for $x_m=0.5$ and $\alpha=7.1\times10^{-4}$ for $x_m=0.25$. The results for $T(x=0,t)$ and $q(x=0,t)$ along the Γ_4 boundary are presented for the three cases in Fig. 10a and b. The GEM solutions are quite impressive, considering the coarse grid of 4 elements or 10 boundary nodes compared to 40 boundary nodes used by Lesnic et al. [6].

3.4. Example 4

This is another transient IHCP with a more stringent test function than Example 3. We use the test function employed by Lesnic et al. [6] that is given by [39]

$$T(x,t)=\begin{cases} u(x,t), & t\in[0,0.5),\\ u(x,t)-2u(x,t-0.5), & t\in[0.5,1),\\ u(x,t)-2u(x,t-0.5)+2u(x,t-1), & t\in[1,1.5),\\ u(x,t)-2u(x,t-0.5)+2u(x,t-1)-2u(x,t-1.5), & t\in[1.5,2], \end{cases} \tag{23}$$

where

$$u(x,t)=\frac{3(1-x)^2-1}{6}+t-2\sum_{n=1}^{\infty}\frac{(-1)^n}{n^2\pi^2}\cos[n\pi(1-x)]e^{-n^2\pi^2t}, \tag{24}$$

Using only 4 rectangular elements as in the previous example, the GEM simulations are carried in a 2-D domain with $\Delta t=0.025$, $\beta=1$ and $\alpha=3.2\times10^{-4}$. The boundary at $x=1$ is a Γ_3 where T and q are specified ($T(x=1,t)$ is obtained from Eq. (23) and $q(x=1,t)=0$), and temperature measurements are available at $x_m=0.25$. The GEM and exact solutions along $x=0$ where neither T nor q is specified are presented in Fig. 11a and b. As in the previous example, the GEM, with this coarse spatial grid, correctly predicts the temperature and heat flux at the boundary where they are not specified.

3.5. Example 5

This is a transient IHCP in which the recovery of the strength of the heat source is sought. It is an example that had previously been addressed by Yan et al. [13] using the method of fundamental solutions (MFS). The exact solution to Eq. (1) in 1-D spatial domain $x\in[0,1]$ is

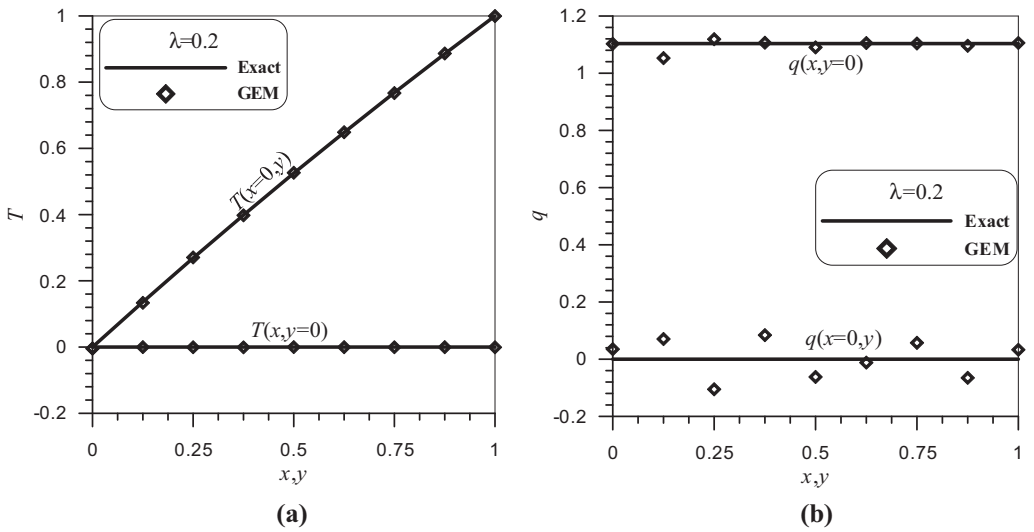

Fig. 8. Numerical solutions for temperature and flux along the Γ_4 boundaries for Example 2, $\lambda=0.2$.

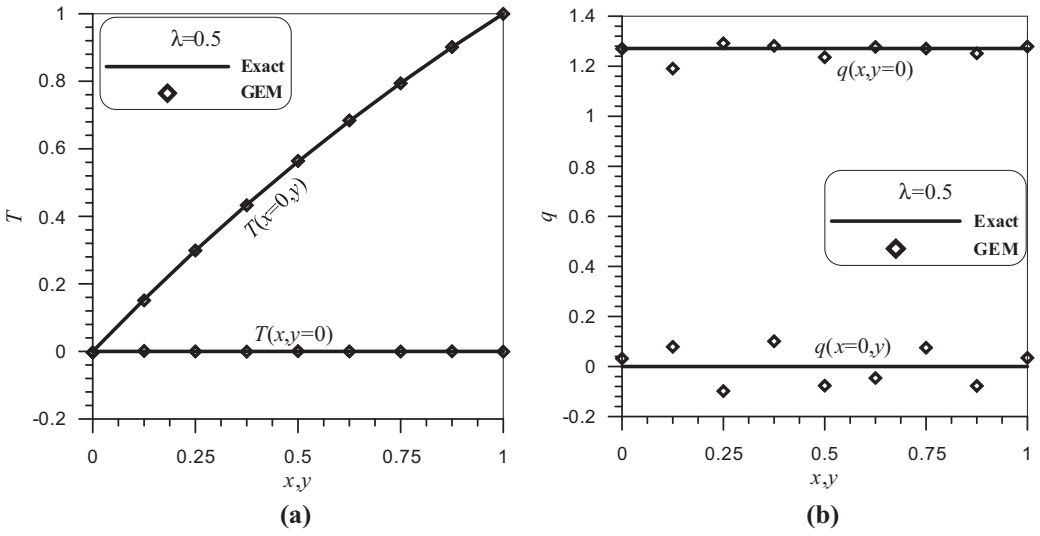

Fig. 9. Numerical solutions for temperature and flux along the Γ_4 boundaries for Example 2, $\lambda = 0.5$.

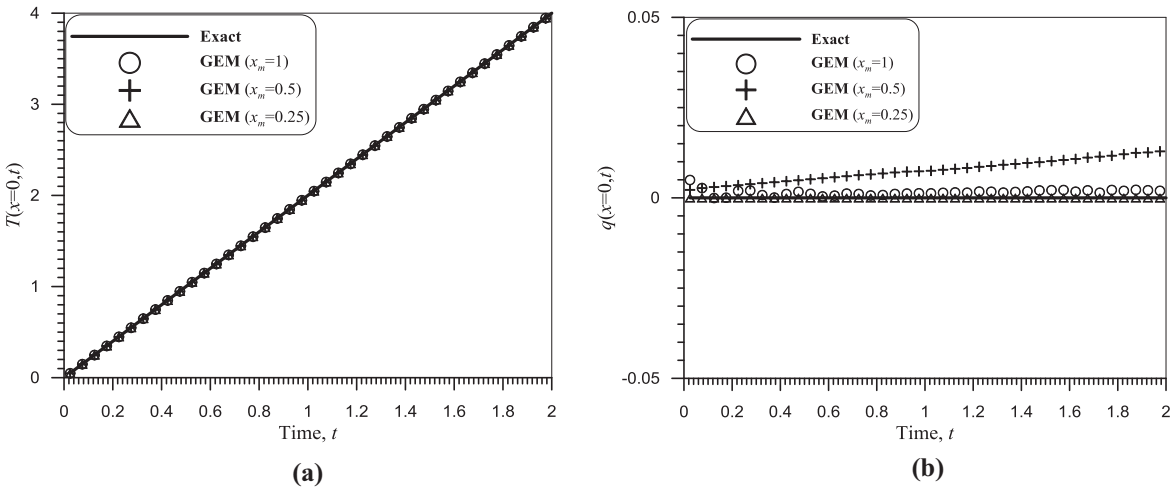

Fig. 10. GEM solutions along $x = 0$ for Example 3; (a) $T(x = 0, t)$ and (b) $q(x = 0, t)$.

$$T(x,t) = \frac{x^4}{4} + 3tx^2 + \sin(x)e^{-t}. \tag{25}$$

With the expression for the heat source being

$$Q(t) = -6t. \tag{26}$$

Dirichlet boundary conditions, obtained from Eq. (25), are specified along $x = 0$ and $x = 1$, while temperature measurements are available at $x_m = 0.5$ for all times. The GEM simulations are carried using 10 linear rectangular elements with no-heat flux boundaries along $y = 0$ and $y = 10^3$. A uniform time step of 0.025 and the fully implicit time differencing scheme $\beta = 1$ are incorporated in the GEM simulations. The temperature data at $x = 0$, 0.5 and 1 are perturbed randomly with noise levels of $\sigma = 1\%$, 3% and 5%. The GEM solutions for the heat source are presented in Fig. 12 for various noise levels. The values of the regularization parameter α used in the GEM simulations are 2.2×10^{-4} for $\sigma = 0\%$ and 3.2×10^{-4} for the other noise levels $\sigma = 1\%$, 3% and 5%. The GEM solutions give a good prediction of the heat source strength at noise levels of 1% and 3% but oscillate about the exact solution at noise level of 5%.

Comparisons between the GEM and exact solutions were done for the temperature along $x = 0.3$ and the heat flux along $x = 0$ by presenting these solutions in Fig. 13a and b. The oscillations of the GEM solution about the exact were significantly pronounced at the noise level of 5%.

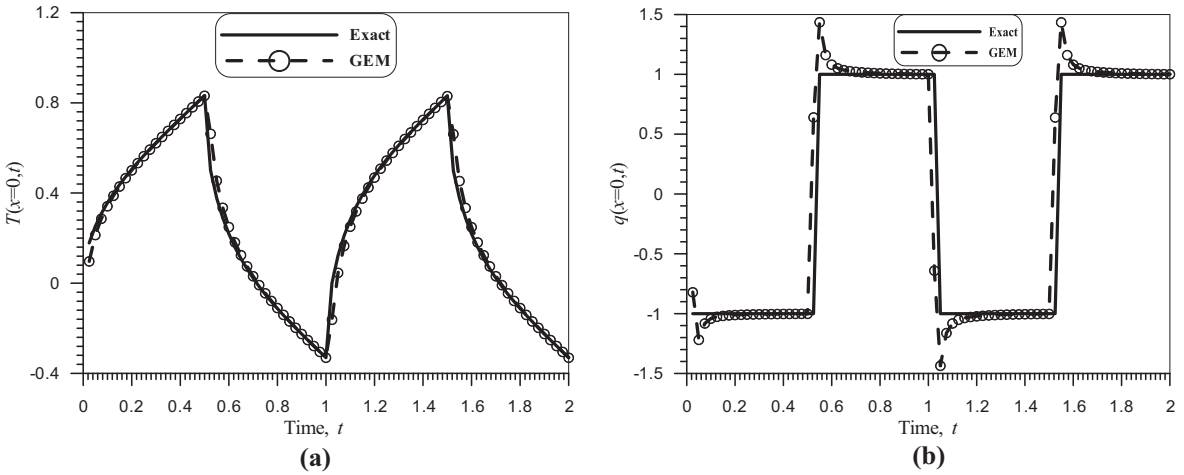

Fig. 11. GEM solutions along $x = 0$ for Example 4; (a) $T(x = 0, t)$ and (b) $q(x = 0, t)$.

3.6. Example 6

This is another transient IHCP previously addressed by Yan et al. [13] using the MFS. The distribution of the heat source is more complicated than the previous example. The expression for the temperature distribution which satisfies Eq. (1) in 1-D spatial domain $x \in [0, 1]$ is

$$T(x,t) = x^2 + 2t + \sin(2\pi t). \tag{27}$$

The functional relationship for the heat source is

$$Q(t) = 2\pi \cos(2\pi t). \tag{28}$$

Along $x = 0$ and $x = 1$ the temperature, obtained from Eq. (27), is specified, and temperature measurements are available at $x_m = 0.5$ for all times. The GEM simulations use 10 linear rectangular elements with no-heat flux boundaries along $y = 0$ and $y = 10^3$, a uniform time step $\Delta t = 0.025$ and a difference weighting $\beta = 1$. The temperature data at $x = 0$, 0.5 and 1 are perturbed randomly with noise levels of $\sigma = 1\%$, 3% and 5%. The GEM and exact solutions for the heat source are presented in Fig. 14 for various noise levels. In the GEM simulations, the values of the regularization parameter are $\alpha = 2.2 \times 10^{-4}$ for $\sigma = 0\%$ and $\alpha = 3.2 \times 10^{-4}$ for the other three noise levels of 1%, 3% and 5%. The GEM results correctly reproduce the exact

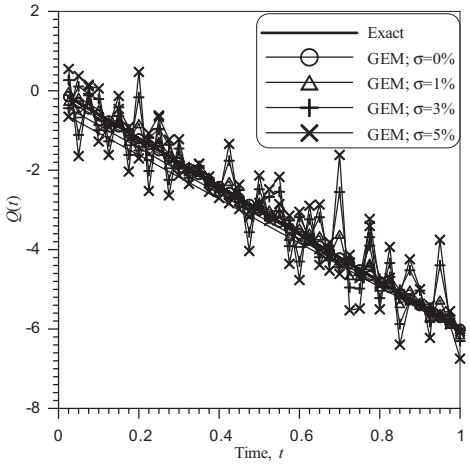

Fig. 12. Recovery of the heat source at various noise levels for Example 5.

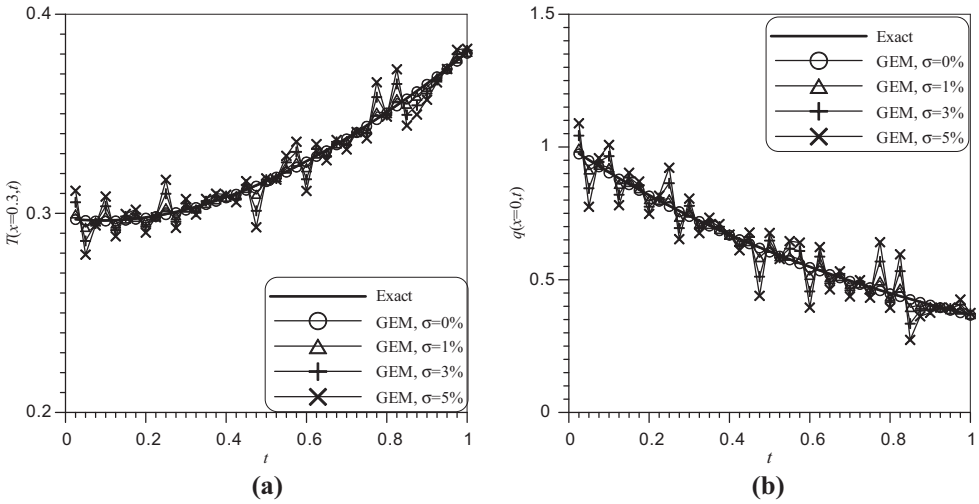

Fig. 13. GEM and exact solutions for Example 5; (a) $T(x = 0.3, t)$, (b) $q(x = 0, t)$.

solution, with subdued oscillations compared to those of Example 5. The GEM and exact solutions for the temperature at $x = 0.3$ and the flux at $x = 0$ are plotted in Fig. 15. The GEM solution for the temperature is virtually oscillation free, but not for the flux when the noise levels are 3% and 5%.

3.7. Example 7

In this example, also previously simulated by Yan et al. [13] using the MFS, the IHCP is governed by Eq. (1) in a 1-D homogeneous domain $x \in [0, 1]$ and solved with zero temperature specified at both ends of the domain. Initially the temperature is zero everywhere in the domain, and the IHCP is to recover the step-wise heat source distribution expressed as:

$$Q(t) = \begin{cases} -1, & t \in [0, 0.25), \\ 1, & t \in [0.25, 0.5) \\ -1, & t \in [0.5, 0.75), \\ 1, & t \in [0.75, 1]. \end{cases} \tag{29}$$

In the absence of an analytic solution, the temperature distribution is generated by solving the direct problem with GEM using fine spatial and temporal discretizations of 40 linear rectangular elements and time step $\Delta t = 2.5 \times 10^{-3}$ in order to

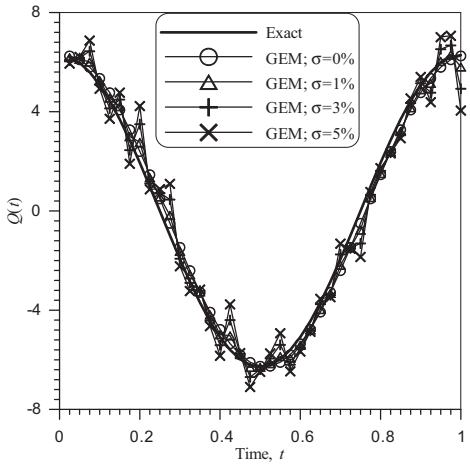

Fig. 14. Recovery of the heat source at various noise levels for Example 6.

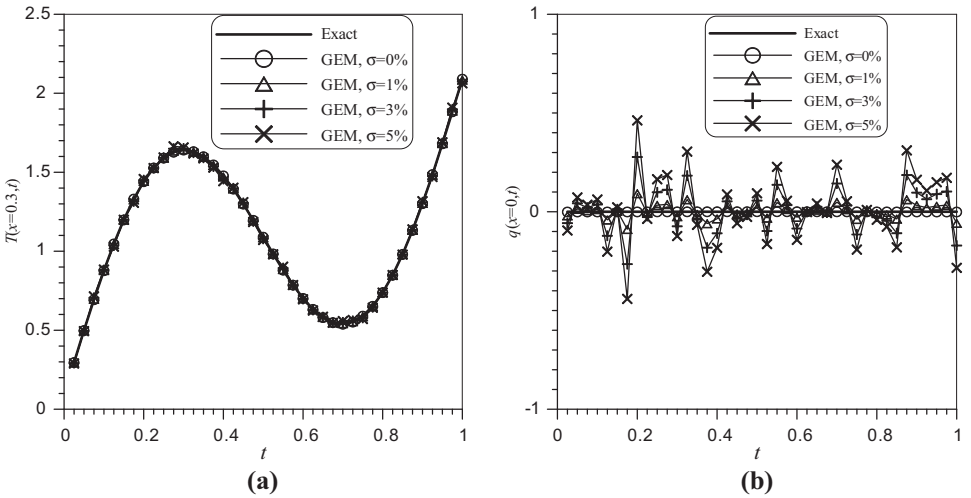

Fig. 15. GEM and exact solutions for Example 6; (a) $T(x = 0.3, t)$, (b) $q(x = 0, t)$.

enhance the accuracy of the solution. The generated direct GEM solution is presented in Fig. 16a, with the temperature at $x_m = 0.5$, used in the inverse modeling, shown in Fig. 16b.

The inverse modeling with GEM is carried out using the specified boundary conditions ($T(x = 0, t) = T(x = 1, t) = 0$), the initial condition ($T(x, 0) = 0$), the temperature data at $x_m = 0.5$ that were generated by the direct GEM (Fig. 16b). Ten linear rectangular elements are used in the inverse GEM simulations with no-heat flux boundaries imposed along $y = 0$ and $y = 10^3$. A uniform time step $\Delta t = 2.5 \times 10^{-2}$ and the fully implicit time differencing scheme $\beta = 1$ are used in the GEM simulations. Because of the homogeneous boundary conditions, only the temperature data at $x = 0.5$ are affected when they are randomly perturbed with noise levels $\sigma = 1\%$, 3% and 5%. The GEM solutions for the heat source are presented in Fig. 17 for various noise levels. The values of the regularization parameter employed in the GEM simulations are 2.2×10^{-4} for $\sigma = 0\%$ and 3.2×10^{-4} for $\sigma = 1\%$, 3% and 5%. The numerical results are excellent for all noise levels, considering the coarse discretization that is used to recover this discontinuous heat source. These results are superior to those obtained by Yan et al. [13] who used the method of fundamental solutions, and the inverse GEM solutions are oscillation-free for all noise levels.

Fig. 18 shows the numerical solutions for the temperature at $x = 0.3$ and the flux at $x = 0$ (the same as the flux at $x = 1$ because of the symmetry of the problem about $x = 0.5$) obtained by the direct and inverse GEM simulations. There is excellent agreement between both numerical solutions.

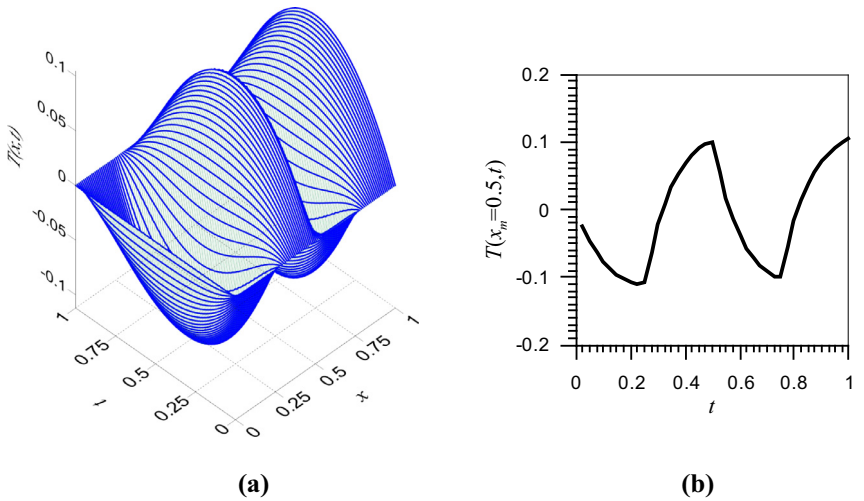

Fig. 16. Direct GEM solutions for Example 7; (a) $T(x, t)$, (b) $T(x_m = 0.5, t)$.

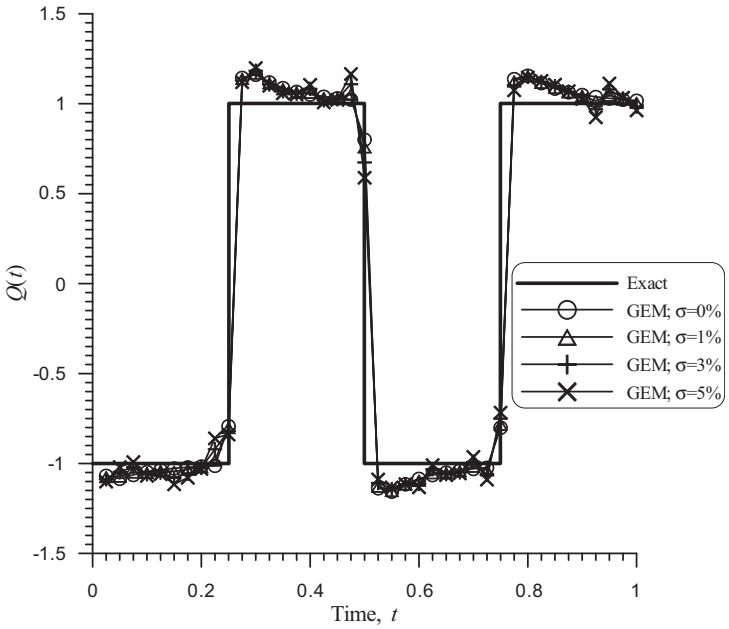

Fig. 17. Recovery of the heat source at various noise levels for Example 7.

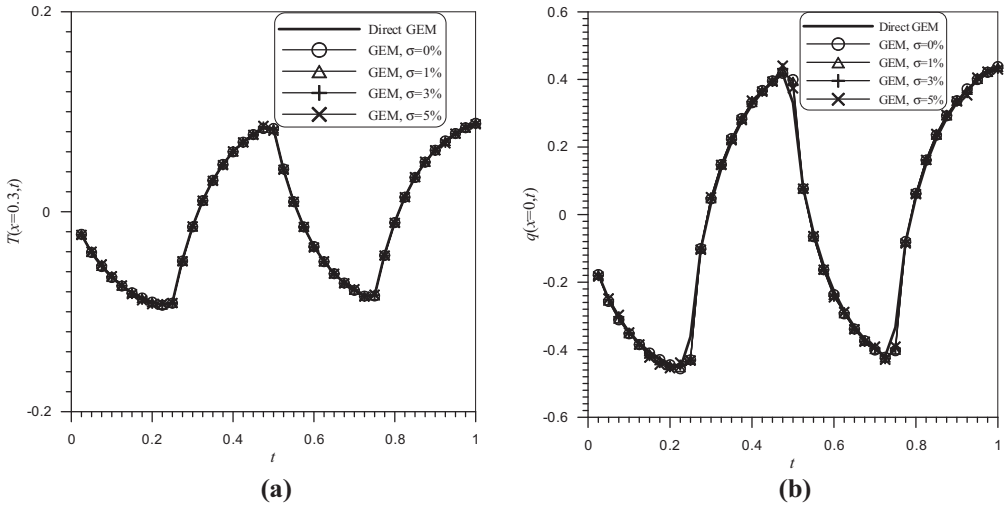

Fig. 18. Direct and inverse GEM solutions for Example 7; (a) $T(x = 0.3, t)$, (b) $q(x = 0, t)$.

4. Conclusions

Using seven numerical examples, we have demonstrated the robustness and accuracy of the recent formulation of the GEM for the solution of steady and transient inverse heat conduction problems in 2-D homogeneous and heterogeneous domains. The two classes of inverse heat conduction addressed are the recovery of the boundary temperature and heat flux, and that of the time-dependent heat source strength that is spatially uniform. The Tikhonov regularization and the SVD technique are used to support the least square solution of the over-determined, ill-condition system of discrete equations that arise from implementing the singular integrals over the elements. It is also demonstrated that the L-curve can facilitate the choice of the regularization parameter. High accuracy of the GEM solutions is observed with relatively coarse spatial discretization of the domain. The prediction of the temperature field is better handled by GEM than the flux. Furthermore, the results show that the current GEM formulation is capable of accommodating IHCPs in which there is noise in the input data.

Acknowledgments

Special thanks go to the National Research Foundation, South Africa which provided partial financial support for this research work.

References

[1] M.J. Ciałkowski, K. Grysa, A sequential and global method of solving an inverse problem of heat conduction equation, J. Theor. Appl. Mech. 48 (2010) 111–134.
[2] T.T.M. Onyango, D.B. Ingham, D. Lesnic, Restoring boundary conditions in heat conduction, J. Eng. Math. 62 (2008) 85–101.
[3] H.J. Reinhardt, D.N. Hao, J. Frohne, F.T. Suttmeier, Numerical solution of inverse heat conduction problems in two spatial dimensions, J. Inverse Ill-posed Prob. 15 (2007) 181–198.
[4] J. Sladek, V. Sladek, Y.C. Hon, Inverse heat conduction problems by meshless local Petrov–Galerkin method, Eng. Anal. Boundary Elem. 30 (2006) 650–661.
[5] Y.C. Hon, T. Wei, A fundamental solution method for inverse heat conduction problem, Eng. Anal. Boundary Elem. 28 (2004) 489–495.
[6] D. Lesnic, L. Elliot, D.B. Ingham, Application of the boundary element method to inverse heat conduction problems, Int. J. Heat Mass Transfer 39 (1996) 1503–1517.
[7] M.-I. Char, F.-P. Chang, B.-C. Tai, Inverse determination of thermal conductivity by differential quadrature method, Int. Commun. Heat Mass Transfer 35 (2008) 113–119.
[8] C. Yang, A linear inverse model for the temperature-dependent thermal conductivity determination in one-dimensional problems, Appl. Math. Modell. 22 (1998) 1–9.
[9] C.-H. Huang, J.-Y. Yan, An inverse problem in simultaneously measuring temperature-dependent thermal conductivity and heat capacity, Int. J. Heat Mass Transfer 38 (1995) 3433–3441.
[10] B. Sawaf, M.N. Özisik, Y. Jarny, An inverse analysis to estimate linearly temperature dependent thermal conductivity components and heat capacity of an orthotropic medium, Int. J. Heat Mass Transfer 38 (1995) 3005–3010.
[11] T. Wei, J.C. Wang, Simultaneous determination for a space-dependent heat source and the initial data by the MFS, Eng. Anal. Boundary Elem. 36 (2012) 1848–1855.
[12] C.-H. Huang, J.-X. Li, S. Kim, An inverse problem in estimating the strength of contaminant source for groundwater systems, Appl. Math. Modell. 32 (2008) 417–431.
[13] L. Yan, C.-L. Fu, F.-L. Yang, The method of fundamental solutions for the inverse heat source problem, Eng. Anal. Boundary Elem. 32 (2008) 216–222.
[14] M. Ikehata, An inverse source problem for the heat equation and the enclosure method, Inverse Prob. 23 (2007) 183–202.
[15] B. Jin, L. Marin, The method of fundamental solutions for inverse source problems associated with the steady-state heat conduction, Int. J. Numer. Methods Eng. 69 (2007) 1570–1589.
[16] Y. Fan, D.-G. Li, Identifying the heat source for the heat equation with convection term, Int. J. Math. Anal. 3 (2009) 1317–1323.
[17] L. Yan, F.-L. Yang, C.-L. Fu, A meshless method for solving an inverse spacewise-dependent heat source problem, J. Comput. Phys. 228 (2009) 123–136.
[18] M.N. Ahmadabadi, M. Arab, F.M.M. Ghaini, The method of fundamental solutions for the inverse space-dependent heat source problem, Eng. Anal. Boundary Elem. 33 (2009) 1231–1235.
[19] M. Mierzwiczak, J.A. Kołodziej, Application of the method of fundamental solutions and radial basis functions for inverse transient heat source problem, Comput. Phys. Commun. 181 (2010) 2035–2043.
[20] M. Yamamoto, J. Zou, Simultaneous reconstruction of the initial temperature and heat radiative coefficient, Inverse Prob. 17 (2001) 1181–1202.
[21] K. Masood, S. Messaoudi, F.D. Zaman, Initial inverse problem in heat equation with Bessel operator, Int. J. Heat Mass Transfer 45 (2002) 2959–2965.
[22] S.S. Pereverzyev, R. Pinnau, N. Siedow, Initial temperature reconstruction for nonlinear heat equation: application to a coupled radiative–conductive heat transfer problem, Inverse Prob. Sci. Eng. 16 (2005) 55–67.
[23] N.S. Mera, L. Elliott, D.B. Ingham, Numerical solution of a boundary detection problem using genetic algorithms, Eng. Anal. Boundary Elem. 28 (2004) 405–411.
[24] F. Yang, L. Yan, T. Wei, Reconstruction of the corrosion boundary for the Laplace equation by using a boundary collocation method, Math. Comput. Simul. 79 (2009) 2148–2156.
[25] N.S. Mera, L. Elliott, D.B. Ingham, Detection of subsurface cavities in IR-CAT by a real coded genetic algorithm, Appl. Soft Comput. 2 (2002) 129–139.
[26] C.H. Cheng, M.H. Chang, Shape design for a cylinder with uniform temperature distribution on the outer surface by inverse heat transfer method, Int. J. Heat Mass Transfer 46 (2003) 101–111.
[27] A.E. Taigbenu, Enhancement of the accuracy of the Green element method: application to potential problems, Eng. Anal. Boundary Elem. 35 (2012) 125–136.
[28] V. Popov, H. Power, L. Skerget (Eds.), Domain Decomposition Techniques for Boundary Elements: Application to Fluid Flow, Wit Press, Southampton, UK, 2007.
[29] A.E. Taigbenu, The Green Element Method, Kluwer, Boston, USA, 1999.
[30] R. Pecher, S.D. Harris, R.J. Knipe, L. Elliot, D.B. Ingham, New formulation of the Green element method to maintain its second-order accuracy in 2D/3D, Eng. Anal. Boundary Elem. 25 (2001) 211–219.
[31] A.E. Taigbenu, The flux-correct Green element formulation for linear, nonlinear heat transport in heterogeneous media, Eng. Anal. Boundary Elem. 32 (2008) 52–63.
[32] G.H. Golub, V.F. Van Loan, Matrix Computations, John Hopkins Univ. Press, Baltimore, USA, 1996.
[33] A.N. Tikhonov, V.Y. Arsenin, Solutions of Ill-posed Problems, Winston and Sons, Washington, USA, 1977.
[34] P.C. Hansen, Regularization tools: a Matlab package for analysis and solution of discrete ill-posed problems, Numer. Algorithms 6 (1994) 1–35.
[35] N. Al-Khalidy, A general space marching algorithm for the solution of two dimensional boundary inverse heat conduction problems, Numer. Heat Transfer, Part B: Fundam.: Int. J. Comp. Meth. 34 (1998) 339–360.
[36] K. Miller, Least squares methods for ill-posed problems with a prescribed bound, SIAM J. Math. Anal. 1 (1970) 52–74.
[37] L.Y. Chen, J.T. Chen, H.-K. Hong, C.H. Chen, Application of Cesàro mean and the L-curve for the deconvolution problem, Soil Dyn. Earthquake Eng. 14 (1995) 361–373.
[38] A. Zeb, L. Elliott, D.B. Ingram, D. Lesnic, A comparison of different methods to solve inverse biharmonic boundary value problems, Int. J. Numer. Methods Eng. 45 (1999) 1791–1806.
[39] H.S. Carslaw, J.C. Jaeger, Conduction of Heat in Solids, Oxford Univ. Press, UK, 1959.